A&A, 708, A108 (2026)
https://doi.org/10.1051/0004-6361/202558035

Astronomy & Astrophysics

From main-sequence binary to blast: MESA modeling of the double-detonation progenitor PTF1 J2238+7430

Mercedes S. Hernandez[1,⋆], Thomas Kupfer[1,2,⋆], Diogo Belloni[3], and Matthias R. Schreiber[4]

[1] Hamburger Sternwarte, University of Hamburg, Gojenbergsweg 112, 21029 Hamburg, Germany
[2] Department of Physics and Astronomy, Texas Tech University, 2500 Broadway, Lubbock, TX 79409, USA
[3] International Centre of Supernovae (ICESUN), Yunnan Key Laboratory of Supernova Research, Yunnan Observatories, CAS, Kunming 650216, China
[4] Departamento de Física, Universidad Técnica Federico Santa María, Avenida España 1680, Valparaíso, Chile

Received 8 November 2025 / Accepted 1 February 2026

ABSTRACT

Context. Hot subdwarf B (sdB) stars in close binaries with white dwarf (WD) companions are potential progenitors of double-detonation thermonuclear supernovae. The recently discovered system PTF1 J2238+7430 is a candidate for this evolutionary channel, as it hosts a low-mass sdB and a comparatively massive white dwarf in a compact orbit.
Aims. We aim to reproduce the evolutionary history of PTF1 J2238+7430, in which the sdB forms first through stable mass transfer, followed by the formation of the white dwarf through a subsequent common-envelope (CE) phase. Additionally, we seek to constrain the range of initial binary parameters that can lead to such double-detonation progenitors.
Methods. Using the Modules for Experiments in Stellar Astrophysics (MESA), we performed detailed binary evolution simulations from the zero-age main sequence to the present-day configuration. We explored initial stellar masses, orbital periods, and mass-loss fractions, including the effects of angular momentum transfer, tidal synchronization, and gravitational-wave-driven orbital evolution. We derived the post-common envelope binary properties using the standard energy formalism during common envelope evolution.
Results. Our models successfully reproduce the observed properties of PTF1 J2238+7430: a 0.406 $M_\odot$ sdB and a 0.72 $M_\odot$ white dwarf in a 76.34-minute orbit. Stable Roche-lobe overflow of an ∼2.7 $M_\odot$ donor produces the sdB, while the white dwarf forms from the initially less massive companion during an episode of common envelope evolution. We find that the common envelope ejection efficiency must be high ($\alpha_{\rm CE} \approx 0.87$) to match the observed orbit, exceeding the canonical values for similar systems. We further delineate the allowed parameter space for initial binaries that can evolve into sdB+WD systems consistent with double-detonation progenitors. These limits are preliminary; a systematic exploration of all parameters is needed to obtain robust constraints. We highlight the main challenges in our MESA simulations and provide a useful starting point for future work.
Conclusions. Our findings identify promising regions of parameter space for the formation of PTF1 J2238+7430–like systems and provide a foundation for future systematic studies of sdB+WD binaries as potential double-detonation Type Ia supernova progenitors.

Key words. methods: numerical – binaries: general – subdwarfs – supernovae: individual: PTF1 J2238+7430

1. Introduction

Most hot subdwarf B (sdB) stars are the stripped cores of red giants that continue to burn helium in their centers while retaining only a thin hydrogen envelope. With typical masses of about 0.5 $M_\odot$, they represent an advanced evolutionary stage and are most commonly found in close binaries (Heber 1986, 2009, 2016, 2026). Many sdB stars have orbital companions with periods shorter than 10 days (Maxted et al. 2001; Napiwotzki et al. 2004; Schaffenroth et al. 2022). In some extreme cases, orbital periods below one hour have been observed (e.g., Vennes et al. 2012; Geier et al. 2013; Kupfer et al. 2017a,b, 2020a,b). These compact systems are generally thought to form through a common-envelope (CE) interaction, which drastically reduces orbital separation. If the post-common envelope orbital period is shorter than about two hours, the sdB is expected to fill its Roche lobe while still undergoing core helium burning (Bauer & Kupfer 2021). Gravitational radiation drives the system toward tighter orbits, typically at periods between 30 and 100 minutes (e.g., Savonije et al. 1986; Tutukov & Fedorova 1989; Tutukov & Yungelson 1990; Iben & Tutukov 1991; Yungelson 2008; Piersanti et al. 2014; Brooks et al. 2015; Neunteufel et al. 2019; Bauer & Kupfer 2021).

These binaries are of particular astrophysical significance because they provide potential progenitors for thermonuclear explosions through the double-detonation channel. In this scenario, the sdB transfers helium-rich matter onto the surface of its white dwarf (WD) companion. If the accumulated helium layer reaches a critical mass, it can ignite unstably. This ignition can trigger either a secondary detonation in the white dwarf core, producing a classical double-detonation supernova even below the Chandrasekhar limit (e.g., Livne 1990; Livne & Arnett 1995; Liu et al. 2023; Fink et al. 2010; Woosley & Kasen 2011; Wang & Han 2012; Shen & Bildsten 2014; Wang 2018; Rajamuthukumar et al. 2025), or cause only a surface helium detonation, giving rise to a faint and rapidly evolving supernova Type Ia event, possibly followed by weaker helium flashes (Bildsten et al. 2007; Brooks et al. 2015).

From an evolutionary perspective, sdB stars generally form through three distinct channels. The second common envelope

⋆ Corresponding authors:
mercedes.hernandez.padilla@uni-hamburg.de;
thomas.kupfer@uni-hamburg.de

ejection channel is the primary mechanism responsible for most of the observed compact sdB+WD systems. In this scenario, the sdB progenitor – already orbiting a white dwarf – undergoes a common envelope phase, and the envelope ejection leaves behind a very close binary with short orbital periods ranging from about 0.5 hours to 25 days. The second channel corresponds to stable Roche-lobe overflow (RLOF), which involves stable mass transfer onto a white dwarf companion. Although this channel is considered less likely because it requires a relatively massive white dwarf companion, it would lead to wide binaries with long orbital periods, typically around 1000 days. Finally, the third main formation channel – the merger of two helium white dwarfs produces a single sdB star rather than a binary system. In all cases, the white dwarf forms first during a common envelope episode, while the sdB emerges later through different evolutionary pathways (Han et al. 2002, 2003). However, recent observations suggest that these sequences may not always hold. Two systems have been identified in which the sdB appears to have formed prior to the white dwarf: CD–30°11223, with a 70.5-minute orbital period and a massive white dwarf companion of about 0.75 $M_\odot$ (Vennes et al. 2012; Geier et al. 2013; Deshmukh et al. 2024), and PTF1 J2238+7430, a close binary with a 76 minute orbital period, proposed as a candidate progenitor of a thermonuclear double-detonation supernova (Kupfer et al. 2022).

According to Kupfer et al. (2022), the future evolution of PTF1 J2238+7430 proceeds as follows. Their calculations indicate that the sdB component will initiate mass transfer of its hydrogen-rich envelope in about 6 Myr at a relatively low rate (Bauer & Kupfer 2021). After ∼60 Myr, while the sdB is still undergoing core-helium burning, it is predicted to transfer helium-rich material to the white dwarf companion. This mass transfer episode is expected to lead to the accumulation of a substantial helium layer of ∼0.17 $M_\odot$, which raises the total white dwarf mass to 0.92 $M_\odot$. At this stage, the models predict that the white dwarf will undergo a thermonuclear instability, triggering a detonation that is likely to disrupt the star in a peculiar thermonuclear supernova (Woosley & Kasen 2011; Bauer et al. 2017). However, Piersanti et al. (2024) and Rajamuthukumar et al. (2025) recently suggested that PTF1 J2238+7430 only exhibits several He-flashes and a thermonuclear supernova is prevented.

PTF1 J2238+7430 is particularly remarkable. Although it is a single-lined spectroscopic binary, detailed modeling shows that it consists of a low-mass hot sdB star ($M_{\rm sdB} = 0.383 \pm 0.028\,M_\odot$) and a comparatively massive white dwarf companion ($M_{\rm WD} = 0.725 \pm 0.026\,M_\odot$), yielding a mass ratio of $q = 0.528 \pm 0.020$ (Kupfer et al. 2022). The binary is nearly edge-on ($i \approx 88.4°$) and displays weak white dwarf eclipses, with an orbital period of $P_{\rm orb} = 76.34179(2)$ minutes. By modeling the eclipses, Kupfer et al. (2022) estimate the temperature of the white dwarf to be $26,800 \pm 4600$ K and the radius to be $0.0109\,R_\odot$, consistent with theoretical models of carbon–oxygen white dwarfs (Romero et al. 2019). The sdB star rotates at 185 ± 5 km s^{-1}, consistent with tidal synchronization (Kupfer et al. 2022).

A notable feature of this system is the discrepancy between the evolutionary ages of its two components: the cooling age of the white dwarf is estimated at ∼25 Myr, whereas the sdB age is predicted to be about ∼170 Myr (Kupfer et al. 2022). This tension can be resolved in a formation scenario in which sdB formed first via stable mass transfer, and the white dwarf companion formed second, following a common envelope episode about 25 Myr ago (Ruiter et al. 2010). Kupfer et al. (2022) did not perform a detailed modeling of the evolutionary history. They only proposed that the progenitor of sdB was likely a ∼2 $M_\odot$ main-sequence star based on the sdB mass.

In this work, our aim is to reproduce the evolutionary pathway proposed by Kupfer et al. (2022) and Ruiter et al. (2010), in which the sdB star forms first through a phase of stable mass transfer, followed by the formation of the white dwarf companion during a subsequent common envelope episode. Using detailed simulations with the Modules for Experiments in Stellar Astrophysics (MESA), we trace the system's evolution from the main sequence to its present configuration. Beyond reproducing this specific case, we constrain the parameter space in which progenitors of double-detonation supernovae may arise on the main sequence. We also explore how our models constrain the efficiency of the common envelope phase, a key but still poorly constrained process in binary stellar evolution (Zorotovic et al. 2010; Zorotovic & Schreiber 2022)

2. MESA simulations

We aimed to reproduce the origin of PTF1 J2238+7430 using the MESA tool (version r24.08.1 of the MESA code Paxton et al. 2011, 2013, 2015, 2018, 2019; Jermyn et al. 2023), following the evolutionary framework proposed by Kupfer et al. (2022). For the MESA simulations, the equation of state combines several sources: OPAL (Rogers & Nayfonov 2002), SCVH (Saumon et al. 1995), FreeEOS (Irwin 2012), HELM (Timmes & Swesty 2000), PC (Potekhin & Chabrier 2010), and Skye (Jermyn et al. 2021). Nuclear reaction rates are drawn from a mixure of NACRE (Angulo et al. 1999), JINA REACLIB (Cyburt et al. 2010), and additional tabulated weak reaction rates (Fuller et al. 1985; Oda et al. 1994; Langanke & Martínez-Pinedo 2000). Screening effects are incorporated following the prescription of Chugunov et al. (2007) and based thermal neutrino losses on Itoh et al. (1996). Electron conduction opacities are taken from Cassisi et al. (2007), sourced radiative opacities primarily from OPAL (Iglesias & Rogers 1993, 1996), and calculated high-temperature Compton-scattering-dominated conditions using the formulae of Buchler & Yueh (1976).

2.1. Formation of sdBs through stable mass transfer

The evolutionary scenario for PTF1 J2238+7430 proposed by Kupfer et al. (2022) suggests that the sdB star forms first through stable mass transfer. To ensure this outcome, we chose the initial masses of the main-sequence stars based on the adiabatic response of the donor star. This stability condition is typically satisfied when the initial mass ratio, q_i, is below a critical threshold, $q_{\rm crit}$. For conservative mass transfer involving donors with masses between 1 and 6 $M_\odot$, $q_{\rm crit}$ at the end of the red giant branch (RGB) phase lies between 0.7 and 1 (Ge et al. 2020).

We performed a series of MESA simulations that evolve both components of a binary system initialized at the zero-age main sequence (ZAMS), with initial conditions ranging from 1.8 to 3.5 $M_\odot$ for the sdB progenitor (Arancibia-Rojas et al. 2024, Figure 4), 1.7–3.0 $M_\odot$ for the companion, and orbital periods between 1–50 days. We investigated different values of the mass-loss fraction during stable mass transfer, β, ranging from 0.85 to 0.15 (Lechien et al. 2025). In this prescription, the companion star accretes between 15–85% of the material lost from the donor's envelope.

We performed the simulations using the MESA binary module under the following assumptions. We computed the mass-transfer rate using the Ritter scheme, allowing for stable

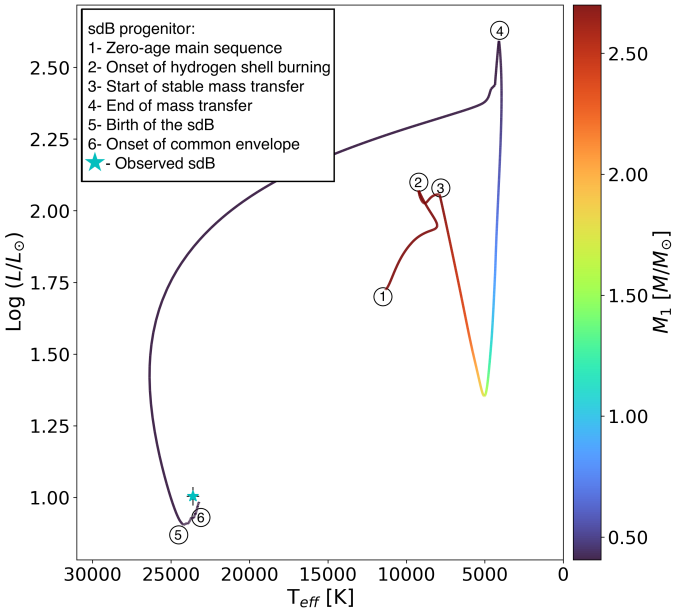

Fig. 1. Evolutionary track of the sdB progenitor calculated with MESA in a binary system with initial stellar masses of 2.7 $M_\odot$ (primary) and 2.6 $M_\odot$ (secondary), and an initial orbital period of 3 days. Point 1 marks the start of the simulation at the zero-age main sequence. Point 2 corresponds to the onset of hydrogen shell burning, while circle 3 indicates the beginning of stable mass transfer, which terminates at point 4 At point 5, the stripped primary becomes an sdB star. Finally, point 6 marks the onset of the common envelope phase initiated by the secondary. The color of the track represents the mass evolution of the primary star. The blue star indicates the observed position of the sdB component of PTF1 J2238+7430, as reported by Kupfer et al. (2022).

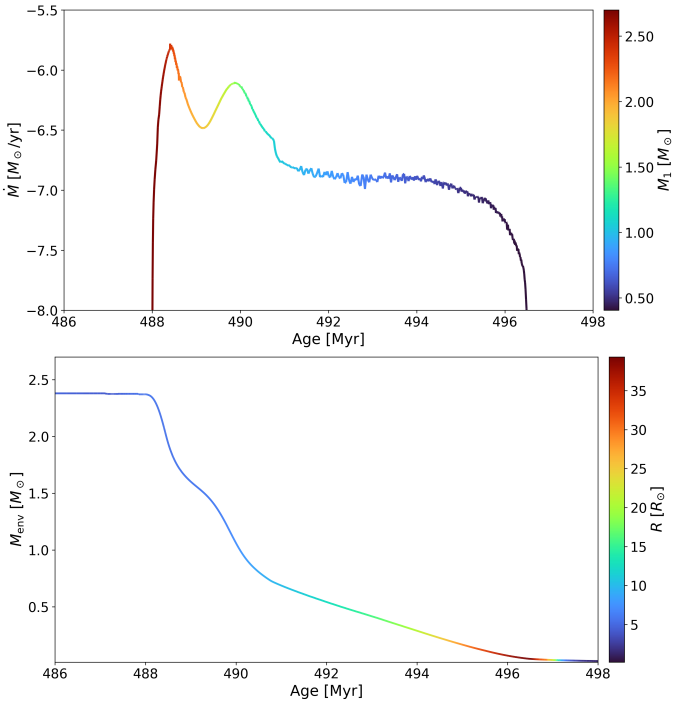

Fig. 2. Evolution of the 2.7 $M_\odot$ main-sequence star during the stable mass-transfer episode. Top: Mass-transfer rate, with colors indicating the change in mass of the sdB progenitor. Bottom: Stripping of the H-rich envelope, with colors indicating the stellar radius as the star evolves to reveal its core (sdB).

Roche-lobe overflow. We adopted nonconservative mass transfer with $\beta > 0$, where β represents the fraction of transferred material accreted by the companion star. The parameters α, δ, and γ describe different modes of angular momentum loss: α through material leaving the vicinity of the accretor, δ through a circumbinary disk, and γ through isotropic reemission or other system-wide outflows. We set all three parameters to zero. We included angular momentum losses from gravitational-wave radiation, systemic mass loss (i.e., mass escaping the binary system entirely and carrying angular momentum away), and spin–orbit coupling, while disabling magnetic braking. We enabled tidal circularization and synchronization, treating both stars as rotating rigid bodies. We allowed wind mass loss and accretion for both components, with a Bondi–Hoyle accretion efficiency of 1.5 and a maximum capture fraction of 1.0.

We evolved the stellar structure at solar metallicity ($Z = 0.02$) using a nuclear network that expanded adaptively as advanced burning stages were encountered. We treated convection via mixing-length theory with $\alpha_{\rm MLT} = 2.0$ (Henyey formulation), applying the Ledoux criterion together with semi-convection (efficiency = 1.0) and thermohaline mixing (coefficient = 2.0). We also included predictive mixing as described in Ostrowski et al. (2021) as well as rotationally induced mixing processes (Solberg-Hoiland, secular shear instability, Eddington-Sweet circulation, Goldreich-Schubert-Fricke, and Spruit-Tayler dynamo) following Heger et al. (2000, 2005). We included convective core overshooting using the exponential prescription with $f = 0.016$ and $f_0 = 0.008$ for $M > 2\,M_\odot$. We modeled mass loss on the RGB and asymptotic giant branch (AGB) with Reimers ($\eta = 0.1$) and Blöcker ($\eta = 0.02$) prescriptions, respectively. To ensure numerical stability during rapid evolutionary phases, such as the helium flash, we applied restrictive timestep and convergence controls. We initialized stellar rotation at 1% of the critical rate for both stars, and allowed the accretor to accrete angular momentum and spin up during stable mass transfer. However, if the breakup limit was reached, we assumed that rotation acts as a regulating mechanism for the mass transfer rate (e.g., Piersanti et al. 2003); that is, the accretor was not allowed to spin up beyond the breakup limit.

We find that the parameters required to successfully reproduce the properties of PTF1 J2238+743 are initial stellar masses of 2.70 $M_\odot$ (donor) and 2.60 $M_\odot$ (accretor), an initial orbital period of 3.0 days, and a mass-loss fraction of $\beta = 0.15$, meaning that 15% of the transferred material is lost from the vicinity of the accretor, carrying its specific angular momentum. The simulation models a close binary system that begins with both stars on the main sequence. The system undergoes a phase of stable Roche-lobe overflow, during which mass is transferred from the initially more massive donor to the secondary. As a result, the donor is stripped of most of its envelope and becomes an sdB star, while the accretor gains mass and eventually becomes a white dwarf.

Figure 1 illustrates the formation of the sdB star through stable mass transfer, as obtained from our MESA simulation, where the 2.7 $M_\odot$ primary is the sdB progenitor. The evolutionary track begins at point 1, when both stars are on the main sequence. After ~487 Myr, the primary evolves into a subgiant, developing a helium core mass of 0.323 $M_\odot$ (point 2). Shortly afterward, at an orbital period of 2.9 days, the primary fills its Roche lobe and initiates stable, non-conservative mass transfer (point 3). Mass transfer initially proceeds on the thermal timescale of the donor, lasting ~2 Myr with rates of order $\dot{M} \sim 10^{-6}\,M_\odot\,{\rm yr}^{-1}$, during

Table 1. Evolution of a zero-age main-sequence binary toward PTF1 J2238+7430.

Time [Myr]	M_1 [$M_\odot$]	M_2 [$M_\odot$]	R_1 [$R_\odot$]	R_2 [$R_\odot$]	Type$_1$	Type$_2$	P_{orb} (days)	Event
0.000	2.700	2.600	1.897	1.859	MS	MS	3.000	zero-age MS binary
487.137	2.699	2.599	4.233	4.063	SG	MS	2.926	change in primary type
487.964	2.699	2.599	5.668	4.076	SG	MS	2.913	onset of stable mass transfer
489.552	1.713	3.437	6.250	3.938	FGB	MS	4.391	change in primary type
496.502	0.406	3.991	39.137	5.058	proto-sdB	MS	157.590	change in primary type (He ignition)
496.612	0.406	3.991	35.228	5.061	proto-sdB	MS	157.863	end of stable mass transfer
529.883	0.405	3.990	0.161	5.850	sdB	MS	158.512	change in primary type
530.585	0.405	3.988	0.161	5.610	sdB	SG	158.606	change in secondary type
533.074	0.405	3.984	0.162	13.852	sdB	FGB	158.904	change in secondary type
533.438	0.405	3.984	0.162	48.586	sdB	CHeB	152.609	change in secondary type
580.092	0.405	3.981	0.172	30.736	sdB	AGB	153.264	change in secondary type
582.134	0.405	3.981	0.173	62.158	sdB	AGB	61.839	onset of CE evolution
582.134	0.405	0.722	0.173	0.594	sdB	proto-WD	0.066	end of CE evolution
583.569	0.405	0.722	0.175	0.044	sdB	WD	0.065	change in secondary type
632.480	0.405	0.722	0.192	0.011	sdB	WD	0.053	binary looks like PTF1 J2238+7430

Notes. MESA evolutions for the pre-common envelope and post-common envelope phases. The terms M_1 and M_2, R_1 and R_2, and Type$_1$ and Type$_2$ indicate the masses, radii, and stellar types of the primary and secondary, respectively The orbital period is defined as P_{orb} and the last column corresponds to the event occurring in the binary at the corresponding time in the first column. The row corresponding to the present-day properties of the binary is highlighted in boldface. Abbreviations: MS (main sequence star), SG (subgiant star), FGB (first giant branch star), CHeB (core helium burning), AGB (asymptotic giant branch star), WD (white dwarf), sdB (hot subdwarf B star), and CE (common envelope).

which the donor loses about 1.0–1.2 $M_\odot$ (top panel of Figure 2). Subsequently, the system enters a longer phase of mass transfer on the nuclear timescale of the donor, at a reduced rate of $\dot{M} \sim 10^{-7}\,M_\odot\,\mathrm{yr}^{-1}$. Roche-lobe overflow ends after ≈9 Myr, at an age of 496.6 Myr. By this time, the envelope of the primary has been nearly stripped away (bottom panel Figure 2), leaving behind a proto-sdB star of 0.406 $M_\odot$ in a binary with an orbital period of 157.9 days (Figure 1 point 4). Helium ignition occurs shortly after, marking the transformation into a core helium-burning sdB star with a residual hydrogen envelope of $M_{env} = 0.0137\,M_\odot$ (Figure 1 point 5 and Figure 2 bottom). Table 1 summarizes all the evolutionary details.

2.2. Formation of the white dwarf through common envelope

Figure 3 illustrates the evolution of the white dwarf progenitor. In the left panel, the system begins as a zero-age main-sequence binary (point 1). At 487.96 Myr, the secondary component (future white dwarf) is still on the main sequence when the primary fills its Roche lobe and stable mass transfer begins (point 2). This episode lasts until 496.61 Myr, at which time the primary has been stripped to a 0.406 $M_\odot$ proto-sdB star and the secondary has accreted mass, reaching 3.99 $M_\odot$ (point 3).

After the end of stable mass transfer, the secondary continues to evolve. At 530.6 Myr it leaves the main sequence and soon after ascends the giant branch, igniting helium in its core. During this phase, the star develops an extended envelope and tidal interactions become significant. The tidal forces act to synchronize the red giant's rotation with the orbital motion, resulting in a gradual reduction of the orbital separation and period (from about 153.264 to 61.839 days) as the star evolves. By 580.1 Myr, the secondary reaches the asymptotic giant branch. At 582.13 Myr, it expands enough to fill its Roche lobe, initiating a second mass-transfer phase that rapidly becomes unstable and triggers a common envelope episode (point 4).

The right panel of Figure 3 shows the binary at the end of the common envelope phase (point 5), when it emerges with an orbital period of 95 minutes and a 0.72 $M_\odot$ proto-white dwarf. By an age of 583.6 Myr, the secondary has contracted and becomes a white dwarf (point 6). We performed a second MESA run starting from this configuration to follow the post-common envelope evolution. In this calculation, we explored different initial orbital periods after envelope ejection and, in parallel, evolved the white dwarf along the cooling track by removing the red giant envelope. By adjusting the post-common envelope orbital period, we obtain a configuration in which, after ∼50 Myr of binary evolution, both the orbital period and the white dwarf effective temperature match the observed properties of PTF1 J2238+7430. At 632.5 Myr, the binary indeed resembles the observed system (marked with a yellow star in Figure 3), consisting of a 0.405 $M_\odot$ sdB and a 0.722 $M_\odot$ white dwarf in a 76.3-minute orbit. The rotational state of the components after the common envelope phase is uncertain; therefore, we did not assume any initial rotation in the post-common envelope sdB+WD model.

Having determined the configuration of the system both before and after the common envelope phase, we were able to calculate the common envelope efficiency using the standard energy formalism of Webbink (1984).

We calculated the envelope binding energy (E_{bind}) by integrating the star envelope from the helium core boundary (i.e., at the radius where the helium mass fraction is 0.1) to the surface of the star, that is,

$$E_{bind} = -\int_{M_{d,c}}^{M_d} \frac{G\,m}{r(m)}\,dm + \int_{M_{d,c}}^{M_d} \varepsilon_{int}(m)\,dm, \quad (1)$$

where the first integral represents the potential energy (E_{grav}), the second represents the internal energy (E_{int}), r is the radius, m is the mass, and ε_{int} is the specific thermodynamic internal energy. Our implementation for computing the thermodynamic internal energy follows Belloni et al. (2024a,b). At the onset of common envelope evolution, $E_{grav} = -1.4641 \times 10^{48}$ erg and $E_{int} = 7.9228 \times 10^{47}$ erg.

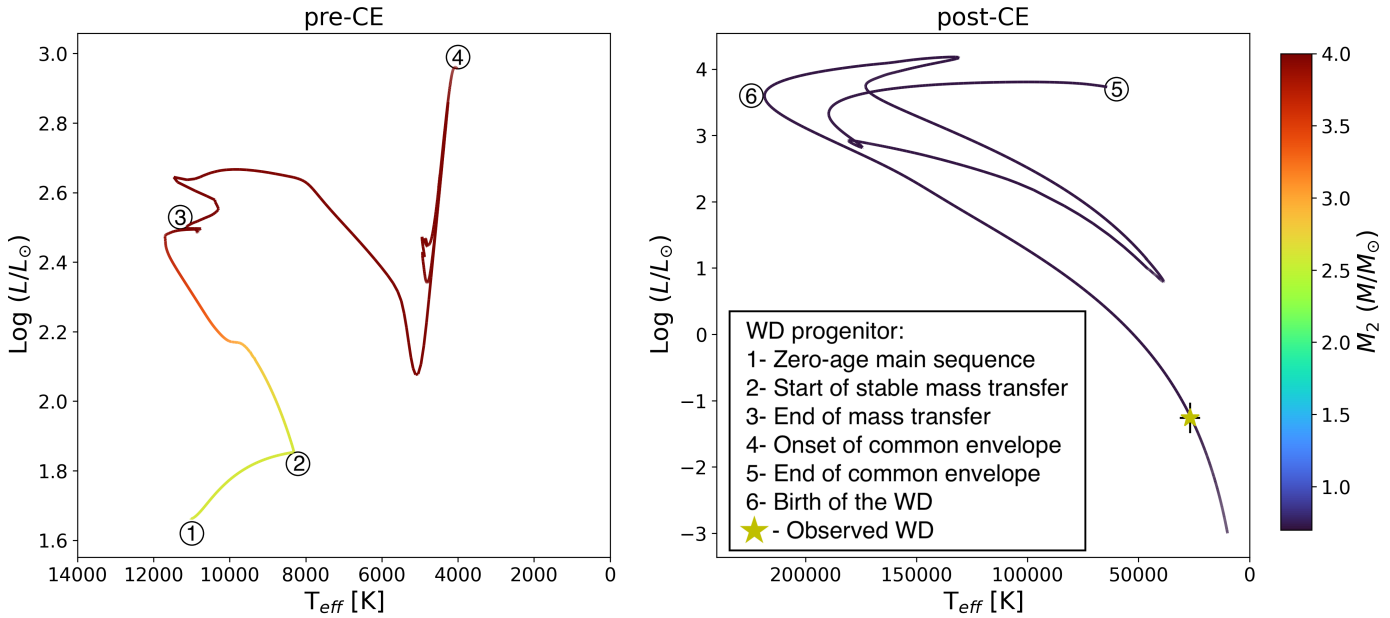

Fig. 3. Evolutionary track of the 2.6 $M_\odot$ star (the white dwarf progenitor) from two MESA simulations. Left: Pre-common envelope evolution, starting at the zero-age main sequence, followed by the onset and termination of stable mass transfer, and culminating in the initiation of the common envelope phase (this corresponds to the same simulation as Figure 1). Right: The white dwarf cooling track was simulated by removing the red giant envelope. The system then emerges as a compact binary, the secondary contracts to form a white dwarf, and the track continues until it reaches the present-day configuration of PTF J2238+7430, marked with a yellow star. In both panels, the color bar indicates the change in the mass of the white dwarf progenitor.

We computed the initial orbital energy from

$$E_{\rm orb,i} = \frac{G\, M_{\rm c,1}\, M_{\rm c,2}}{2\, a_{\rm i}}, \tag{2}$$

where $M_{\rm c,1} = 0.7217\, M_\odot$ is the CO core mass of the primary at the onset of the common envelope, $M_{\rm c,2} = 0.4054\, M_\odot$ is the total mass of the secondary, and $a_{\rm i} = 107.726\, R_\odot$ is the binary separation. For these values, we obtain $E_{\rm orb,i} \approx 3.521 \times 10^{46}$ erg.

The final orbital energy is given by

$$E_{\rm orb,f} = E_{\rm orb,i} - \frac{E_{\rm bind}}{\alpha_{\rm CE}}, \tag{3}$$

where $\alpha_{\rm CE}$ is the CE ejection efficiency. For each assumed $\alpha_{\rm CE}$ in the range $0.0 \leq \alpha_{\rm CE} \leq 1.0$, we calculated the corresponding final orbital separation

$$a_{\rm f} = \frac{G\, M_{\rm c,1}\, M_{\rm c,2}}{2\, E_{\rm orb,f}}, \tag{4}$$

and derived the post-common envelope orbital period from Kepler's third law. This procedure allowed us to map the possible final orbital configurations for the given pre- and post-common envelope parameters. Figure 4 shows the post-common envelope orbital period as a function of the common envelope ejection efficiency. For PTF1 J2238+7430, the observationally inferred post-common envelope period (95 min) corresponds to $\alpha_{\rm CE} \approx 0.87$. Table 2 presents a detailed comparison between the observed properties of PTF1 J2238+7430 and the outcomes of our MESA simulations.

3. Discussion

The solution we obtain for the formation of the observed sdB+WD system represents only one of several possible configurations. Its validity is highly sensitive to the initial assumptions adopted in the simulations. Consequently, the results should be considered illustrative rather than definitive.

3.1. Mass and angular momentum accretion efficiencies

The formation of the sdB+WD binary is based on several key assumptions regarding the physics of mass transfer, each of which introduces uncertainties that may affect the outcome. Although there is no universal prescription for the fraction of mass lost during Roche-lobe overflow episodes (Webbink 2008), we adopted a nonconservative mass transfer scheme in our simulations. Our exploration of the mass-loss fraction (the β parameter) was limited; nevertheless, we find that systems capable of reproducing the observed configuration require highly conservative mass transfer (at least ~85% of the transferred mass accreted by the companion).

This finding is broadly consistent with the results of Lechien et al. (2025). In their sample of 16 stripped stars with rapidly rotating companions (Be+sdOB systems), they report that about half of the binaries required the accretor to retain at least 50% of the transferred mass. Moreover, they show that assuming a constant accretion efficiency – where all secondaries accrete between 60% and 80% of the transferred mass – could, in principle, reproduce the entire sample. However, when analyzing individual systems with configurations similar to PTF1 J2238+7430 (such as 7 Vul and κ Dra), reproducing the observed system characteristics through stable mass transfer can be achieved with substantially lower efficiencies. This suggests that while our adopted assumptions allow us to reproduce the observed system, alternative solutions with different mass-loss fractions may also be viable.

In our modeling, the accretion of matter and angular momentum is drastically reduced once the main-sequence secondary

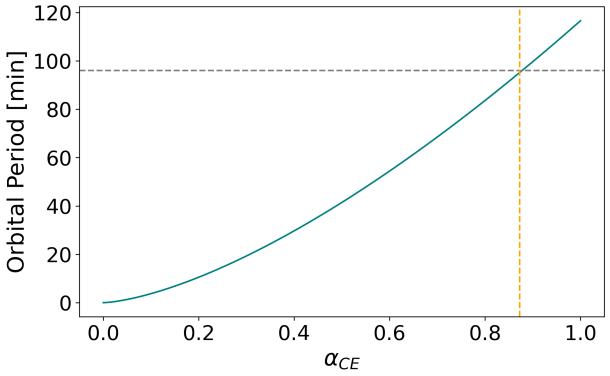

Fig. 4. Common-envelope efficiency ($\alpha_{\rm CE}$) vs. final orbital period. The solid line indicates the possible post-common envelope orbital configurations. The horizontal dashed line indicates the predicted orbital period of 95.04 minutes for PTF1 J2238+7430 (Kupfer et al. 2022), while the vertical dashed orange line marks the corresponding $\alpha_{\rm CE} = 0.872$. The recombination energy was fixed to $\lambda = 1$.

Table 2. Observational constraints vs. MESA models for PTF1 J2238+7430.

Parameter	Observed	Simulation
$P_{\rm orb}$ [min]	76.34179(2)	76.330
$M_{\rm sdB}$ [$M_\odot$]	0.383 ± 0.028	0.405
$M_{\rm WD}$ [$M_\odot$]	0.725 ± 0.026	0.722
$R_{\rm sdB}$ [$R_\odot$]	0.190 ± 0.003	0.192
$R_{\rm WD}$ [$R_\odot$]	0.0109 ± 0.0003	0.011
$T_{\rm eff,sdB}$ [K]	$23{,}600 \pm 400$	23,190
$T_{\rm eff,WD}$ [K]	$26{,}800 \pm 4{,}600$	24,045
log $g_{\rm sdB}$	5.42 ± 0.06	5.477
log $g_{\rm WD}$	–	8.213
Age$_{\rm sdB}$ [Myr]	170	104.316
Age$_{\rm WD}$ [Myr]	25	50.35

Notes. Comparison between the observational constraints of PTF1 J2238+7430 reported by Kupfer et al. (2022, KT22) and the results of our MESA simulations. The table lists the main stellar and orbital parameters used as benchmarks.

reaches the breakup spin; that is, it accretes only the amount required to maintain rotation at the breakup limit. In principle, limiting angular momentum accretion during mass transfer is justified, since tidal forces eventually synchronize the accretor's rotation with the orbit after mass transfer. However, if matter continues to accrete after the accretor reaches the breakup velocity, with excess angular momentum returned to the accretion disk as suggested by Paczynski (1991) and Popham & Narayan (1991), we believe that a reasonable model for PTF1 J2238+7430 remains possible with different initial masses and orbital periods. That being said, exploring different assumptions for angular-momentum transport in future simulations will be useful for further further testing the robustness of these results.

To assess the impact of rotation on the system properties, we performed an additional simulation with the same initial parameters and mass-transfer efficiency as our best-fitting model, but neglecting rotational effects throughout the evolution. We find that the resulting sdB star is slightly cooler, more luminous, larger, and retains a marginally thicker hydrogen envelope. However, these differences remain within the observational uncertainties, indicating that in this case, rotation has only a minor effect on the final system properties.

3.2. Common envelope efficiency assumptions

Our main objective was to identify a binary configuration that could reproduce the observed properties of PTF1 J2238+7430 upon evolution. The guiding hypothesis was that such a configuration, after undergoing common envelope evolution, would require an efficiency parameter of $\alpha_{\rm CE} \simeq 0.2{-}0.4$, based on values inferred for post-common envelope binaries hosting AFGKM stars with white dwarf companions (Zorotovic et al. 2010; Hernandez et al. 2021, 2022a,b; Zorotovic & Schreiber 2022).

However, we found that achieving such low values of $\alpha_{\rm CE}$ requires that the binary retains an orbital period of at least ~400 days immediately after the phase of stable mass transfer. In contrast, across all models explored, the longest orbital period obtained after stable mass transfer was only ~170 days, significantly below the required minimum. This discrepancy suggests that the common envelope efficiency in PTF1 J2238+7430 must have been substantially higher than the canonical range typically adopted for other post-common envelope systems, assuming full recombination energy efficiency ($\lambda = 1$). This result is consistent with Zhang et al. (2024), who report that common envelope efficiencies tend to be higher for systems with more massive white dwarf progenitors.

Alternatively, discrepancies in the derived values of $\alpha_{\rm CE}$ between PTF1 J2238+7430 and systems containing AFGKM stars with white dwarf companions may result from fundamental differences in their evolutionary histories. Most empirical constraints on the common envelope efficiency parameter are based on binaries in which the common envelope phase corresponds to the first episode of mass transfer. In contrast, for PTF1 J2238+7430 the common envelope phase corresponds to the second mass-transfer event, following an earlier phase of stable Roche-lobe overflow. According to Ge et al. (2024), this distinction may play a key role in explaining the higher efficiency required in PTF1 J2238+7430. In contrast, Nelemans et al. (2025) show that the first phase of mass transfer in low-mass systems often proceeds neither as stable mass transfer nor as a common envelope phase. Therefore, if the physics of stable mass transfer is not fully understood, our constraints on $\alpha_{\rm CE}$ remain uncertain. In future work, implementing an explicit treatment of the recombination efficiency in MESA, following for example the approach of Belloni et al. (2025), could allow us to derive tailored common envelope efficiencies that depend on the internal structure of each stellar model.

Although our simulations successfully identified a configuration that reproduces the observed properties of PTF1 J2238+7430, a major difficulty arises when attempting to obtain sufficiently long post-stable mass-transfer orbital periods (>400 days) consistent with low values of $\alpha_{\rm CE}$. A possible pathway to reach longer orbital periods could involve the enhanced wind prescription recently proposed by Gao & Li (2023), which increases orbital separation prior to the onset of mass transfer. Nevertheless, for PTF1 J2238+7430, this mechanism would only be viable for initially massive main-sequence stars, since the large amounts of mass lost through the wind would otherwise prevent the formation of a sufficiently massive white dwarf ($M_{\rm WD} \gtrsim 0.7\,M_\odot$). This limitation highlights that, under the present assumptions of solar metallicity and suppressed angular momentum accretion, the enhanced wind channel cannot fully reconcile the observed properties of the system.

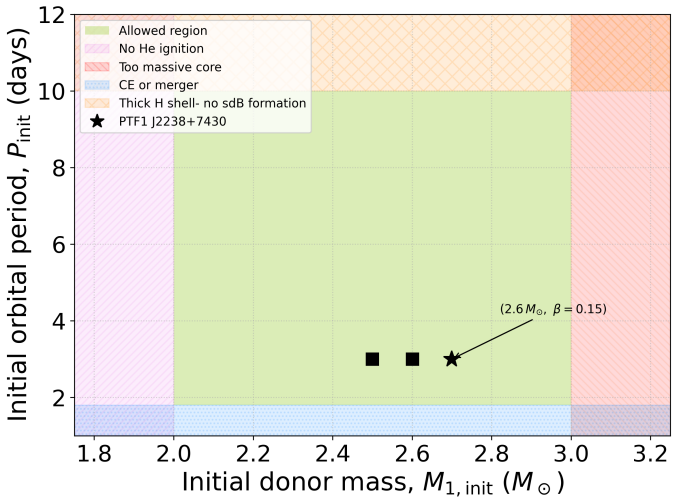

Fig. 5. Allowed and excluded regions for the formation of an sdB+WD binary through stable mass transfer similar to PTF1 J2238+7430. The central green-shaded region indicates combinations of initial donor mass ($M_{1,\rm init}$) and orbital period ($P_{\rm init}$) that lead to sdB formation consistent with observations. The hatched and colored regions correspond to physically forbidden configurations: violet (left) shows donors too low in mass (no He ignition); red (right) shows donors too massive (oversized core or Roche-lobe overflow in the subgiant phase); blue (bottom) shows systems at risk of common envelope or merger events; and orange (top) shows donors with thick hydrogen shells preventing sdB formation. The black star marks PTF1 J2238+7430 parameters, while black squares mark model systems that produced potential double-detonation supernova progenitors with slightly different masses from the observed system.

However, the existence of other long-period sdB+WD binaries with comparable component masses, such as those illustrated in Garbutt et al. (2024, their Fig. 8), suggest that alternative evolutionary pathways or additional physical ingredients may provide multiple viable solutions. Future work should therefore explore these possibilities, including systematic variations in metallicity, angular momentum accretion prescriptions, and mass-loss mechanisms, to better constrain the range of evolutionary channels that could lead to PTF1 J2238+7430–like systems.

3.3. Parameter range for similar evolutionary pathways

Although our simulations explore a wide range of parameters (see appendix Table A.1), we did not carry them out in a fully systematic manner. Consequently, the trends and limits that we identify should be regarded as preliminary indications of the parameter space that appears promising for forming systems similar to PTF1 J2238+7430, rather than as strict constraints.

Producing a long-period post-stable mass transfer sdB+WD binary requires a delicate balance between the component masses and the initial orbital period. A mass ratio close to unity ($q \approx 1$) is essential to maintain stability during Roche-lobe overflow, while the donor mass (M_1) plays a particularly central role. For $M_1 \gtrsim 3$–$3.5\,M_\odot$, the hydrogen-free core mass at the onset of mass transfer tends to exceed the observed sdB mass, implying that sdB formation would requires Roche-lobe overflow during the sub-giant phase (Arancibia-Rojas et al. 2024), which generally produces post-stable mass transfer orbital periods shorter than observed. Overshooting effects in this regime also tend to yield sdB masses larger than those measured in PTF1 J2238+7430. While more massive sdB stars are not problematic in a general evolutionary context, reproducing the specific properties of PTF1 J2238+7430 requires forming a relatively low-mass core in the range $\sim$0.36–0.41 $M_\odot$. At the other extreme, for $M_1 \lesssim 1.8\,M_\odot$, two issues arise. First, helium ignition does not occur at the observed sdB mass in red giants with degenerate cores, preventing sdB formation of the required mass. Second, even for $M_1 \approx 1.8\,M_\odot$, the resulting white dwarf progenitor mass after conservative mass transfer is typically too low ($\lesssim$3.6 $M_\odot$), preventing the formation of a white dwarf with $M \gtrsim 0.7\,M_\odot$. Taken together, these trends suggest that viable progenitors are more likely to be found around $M_1 \sim 2$–$3\,M_\odot$, with roughly equal-mass binaries ($M_1 \approx M_2 \approx 2$–$3\,M_\odot$) appearing particularly favorable for reproducing both the observed masses and the orbital period.

The initial orbital period ($P_{\rm orb,init}$) also shows a strong influence. For periods much longer than $\sim$10 days, helium ignition may occur before the end of stable mass transfer, preventing sdB formation because a significant fraction of the donor mass has not yet been processed into the helium core. In addition, in this regime the donor can retain a more massive hydrogen envelope than the typical $\sim 3.16 \times 10^{-5}$–0.01 $M_\odot$ found in sdB stars (Bauer & Kupfer 2021; Arancibia-Rojas et al. 2024; Rodríguez-Segovia et al. 2025), further complicating the reproduction of the observed system. Conversely, very short initial periods (a few days or less) tend to produce post mass-transfer orbits that are overly compact, increasing the risk of Roche-lobe overflow by the accretor, which may drive the system into a common envelope phase instead of stable mass transfer, or even lead to a merger. In addition, higher M_1 values generally require shorter $P_{\rm orb,init}$ to keep the hydrogen-free core mass low, which in turn favors higher mass-loss fractions (β) to avoid excessive accretor growth. These interdependencies highlight the delicate balance between the different parameters in reproducing the observed system.

The fraction of mass lost from the system during Roche-lobe overflow, denoted β, also plays a critical role in the evolution of the binary. Very low values of β ($\beta \lesssim 0.15$) lead to excessive accretion onto the secondary, potentially driving it to critical rotation or inducing premature Roche-lobe overflow. In contrast, very high values ($\beta \gtrsim 0.85$–0.90) hinder sufficient core growth in the donor before the envelope is removed, preventing helium ignition. Our simulations indicate that only an intermediate range of β ($\sim$0.15–0.85) allows for formation of viable sdB stars.

Figure 5 summarizes the regions of the initial parameter space, particularly the donor mass ($M_{1,\rm init}$) and the orbital period ($P_{\rm init}$). The large green-shaded square represents combinations of $M_{1,\rm init}$ and $P_{\rm init}$ that potentially correspond to initial configurations of post-stable mass-transfer systems. These configurations lead to the formation of sdB+WD binaries consistent with the observational constraints of PTF1 J2238+7430, assuming $q_{\rm crit} \gtrsim 1$ and $\beta = 0.15$. This parameter space may help identify systems similar to PTF1 J2238+7430, such as those marked with black squares, which contain an sdB and a white dwarf with minimum masses of $\sim$0.4 $M_\odot$ and $\sim$0.7 $M_\odot$, respectively. These masses are sufficient to consider them as potential progenitors of double-detonation Type Ia supernovae (Livne 1990; Livne & Arnett 1995; Fink et al. 2010; Woosley & Kasen 2011; Wang & Han 2012; Wang 2018; Shen & Bildsten 2014). Overall, these constraints provide a useful guide and foundation for more systematic future explorations of the parameter space.

In summary, while our models identify a plausible parameter space for reproducing the observed system, they rely on a

series of tightly constrained assumptions, and our exploration of the initial parameter space remains preliminary and should be regarded as indicative rather than exhaustive. Slight deviations in component masses, initial orbital period, or mass-transfer efficiency can prevent the formation of the observed sdB+WD binary, emphasizing the sensitivity of these evolutionary pathways. We did not include element diffusion (i.e., gravitational settling and chemical diffusion) in our models. Since diffusion can modify the predicted values of $\log g$ and $T_{\rm eff}$, its inclusion would likely require a slightly different initial primary mass to reproduce the present-day properties of the sdB component (Michaud et al. 2007; Ostrowski et al. 2021). We also did not vary the stellar metallicity, which could in principle affect the internal structure, core growth, and mass-loss rates. Some of these limitations can be alleviated by relaxing the restriction that keeps the common envelope efficiency $\alpha_{\rm CE}$ strictly around 1/3 and instead allowing it to adopt higher values. Future studies should also consider systems with different sdB and white dwarf masses, which could still qualify as potential double-detonation supernova Ia progenitors. Consequently, while our results highlight promising regions of parameter space, further work is needed to map all possible evolutionary channels more rigorously and quantify their likelihood.

Lagos et al. (2020) and Lagos-Vilches et al. (2024) suggest that systems with similar parameters and evolutionary pathways similar to those we inferred for PTF1 J2238+7430 at the main-sequence stage (initial donor mass $M_{1,\rm init} \sim 2.7\,M_\odot$, companion mass $M_{2,\rm init} \sim 2.7\,M_\odot$, and initial orbital period $P_{\rm orb,init} \sim 3$ days) are likely to host a distant tertiary companion. Main-sequence binaries with short orbital periods ($\lesssim$5 days) have a high probability of being part of a hierarchical triple system (Tokovinin et al. 2006). To investigate this possibility, we searched the *Gaia* DR3 catalog for sources around of PTF1 J2238+7430 that have consistent parallax and proper motion values. We find no candidate objects that could plausibly be associated with the system, but a deeper search and/or perhaps higher angular resolution observations are required to exclude the hypothesis that PTF1 J2238+7430 is part of a hierarchical triple.

4. Summary and conclusions

Our simulations reproduce the evolutionary pathway of PTF1 J2238+7430, as originally proposed by Kupfer et al. (2022). Starting from a close binary on the main sequence, we find that stable Roche-lobe overflow of a $\sim$2.7 $M_\odot$ donor produces a stripped helium-burning core that matches the observed sdB properties. The accretor grows in mass, reaching nearly 4 $M_\odot$, and subsequently evolves toward the giant branch. At this stage, unstable mass transfer triggers a common envelope event, leaving behind a 0.406 $M_\odot$ sdB and a 0.72 $M_\odot$ white dwarf in a compact orbit. Gravitational-wave radiation then shrinks the orbit to the present-day configuration, with a cooling age for the white dwarf consistent with observations. By providing an evolutionary model that reproduces the observed parameters, our results provide strong support for the stable mass transfer plus common envelope scenario. Moreover, the derived common envelope efficiency of $\alpha_{\rm CE} \approx 0.87$ highlights the importance of envelope physics in shaping compact binaries and possible progenitors of thermonuclear supernovae.

However, reproducing this system requires finely tuned assumptions. The results are highly sensitive to the values adopted for the mass-loss fraction β, the treatment of angular momentum accretion, and the efficiency of the common envelope phase. We find that explaining PTF1 J2238+7430 requires a relatively high common envelope efficiency ($\alpha_{\rm CE} \approx 0.8$), higher than the canonical values inferred for many other post-common envelope binaries. This difference may reflect the distinct evolutionary history of this system, in which the common envelope corresponds to a second mass-transfer phase rather than the first.

Our results should therefore be viewed as indicative rather than definitive. The parameter space outlined in Figure 5 highlights promising regions for forming systems similar to PTF1 J2238+7430 and may also point to other sdB+WD binaries with component masses sufficient to qualify as potential double-detonation Type Ia supernova progenitors. Furthermore, some areas that we excluded from our analysis, such as progenitors with main-sequence masses >3.0 $M_\odot$, could lead to the formation of more massive sdB stars, which in turn may also represent viable double-detonation supernova progenitors. These regimes should therefore be included in future studies aimed at characterizing the broader population of sdB+WD systems. A more systematic exploration, covering variations in metallicity, angular momentum transport, and mass-loss prescriptions, is necessary to fully map the range of viable evolutionary channels and to assess their relative likelihood within stellar populations. Ultimately, extending this work into population synthesis studies will be key to quantifying the frequency of such systems and evaluating their contribution to the overall Type Ia supernova rate.

Acknowledgements. This research was supported by Deutsche Forschungsgemeinschaft (DFG, German Research Foundation) under Germany's Excellence Strategy – EXC 2121 "Quantum Universe" – 390833306. Co-funded by the European Union (ERC, CompactBINARIES, 101078773). Views and opinions expressed are however those of the author(s) only and do not necessarily reflect those of the European Union or the European Research Council. Neither the European Union nor the granting authority can be held responsible for them. MRS acknowledge financial support from FONDECYT (grant number 1221059). DB acknowledges support from FONDECYT (grant number 3220167) and the São Paulo Research Foundation (FAPESP), Brazil, Process Numbers 2024/03736-2 and 2025/00817-4.

References

Angulo, C., Arnould, M., Rayet, M., et al. 1999, Nucl. Phys. A, 656, 3
Arancibia-Rojas, E., Zorotovic, M., Vučković, M., et al. 2024, MNRAS, 527, 11184
Bauer, E. B., & Kupfer, T. 2021, ApJ, 922, 245
Bauer, E. B., Schwab, J., & Bildsten, L. 2017, ApJ, 845, 97
Belloni, D., Mikołajewska, J., & Schreiber, M. R. 2024a, A&A, 686, A226
Belloni, D., Schreiber, M. R., & Zorotovic, M. 2024b, A&A, 687, A12
Belloni, D., Schreiber, M. R., & El-Badry, K. 2025, A&A, 697, A100
Bildsten, L., Shen, K. J., Weinberg, N. N., & Nelemans, G. 2007, ApJ, 662, L95
Brooks, J., Bildsten, L., Marchant, P., & Paxton, B. 2015, ApJ, 807, 74
Buchler, J. R., & Yueh, W. R. 1976, ApJ, 210, 440
Cassisi, S., Potekhin, A. Y., Pietrinferni, A., Catelan, M., & Salaris, M. 2007, ApJ, 661, 1094
Chugunov, A. I., Dewitt, H. E., & Yakovlev, D. G. 2007, Phys. Rev. D, 76, 025028
Cyburt, R. H., Amthor, A. M., Ferguson, R., et al. 2010, ApJS, 189, 240
Deshmukh, K., Bauer, E. B., Kupfer, T., & Dorsch, M. 2024, MNRAS, 527, 2072
Fink, M., Röpke, F. K., Hillebrandt, W., et al. 2010, A&A, 514, A53
Fuller, G. M., Fowler, W. A., & Newman, M. J. 1985, ApJ, 293, 1
Gao, S.-J., & Li, X.-D. 2023, MNRAS, 525, 2605
Garbutt, J. A., Parsons, S. G., Toloza, O., et al. 2024, MNRAS, 529, 4840
Ge, H., Webbink, R. F., Chen, X., & Han, Z. 2020, ApJ, 899, 132
Ge, H., Tout, C. A., Webbink, R. F., et al. 2024, ApJ, 961, 202
Geier, S., Marsh, T. R., Wang, B., et al. 2013, A&A, 554, A54
Han, Z., Podsiadlowski, P., Maxted, P. F. L., Marsh, T. R., & Ivanova, N. 2002, MNRAS, 336, 449
Han, Z., Podsiadlowski, P., Maxted, P. F. L., & Marsh, T. R. 2003, MNRAS, 341, 669
Heber, U. 1986, A&A, 155, 33
Heber, U. 2009, ARA&A, 47, 211

Heber, U. 2016, PASP, 128, 082001
Heber, U. 2026, in Encyclopedia of Astrophysics, 2, 488
Heger, A., Langer, N., & Woosley, S. E. 2000, ApJ, 528, 368
Heger, A., Woosley, S. E., & Spruit, H. C. 2005, ApJ, 626, 350
Hernandez, M. S., Schreiber, M. R., Parsons, S. G., et al. 2021, MNRAS, 501, 1677
Hernandez, M. S., Schreiber, M. R., Parsons, S. G., et al. 2022a, MNRAS, 512, 1843
Hernandez, M. S., Schreiber, M. R., Parsons, S. G., et al. 2022b, MNRAS, 517, 2867
Iben, I., Jr., & Tutukov, A. V. 1991, ApJ, 370, 615
Iglesias, C. A., & Rogers, F. J. 1993, ApJ, 412, 752
Iglesias, C. A., & Rogers, F. J. 1996, ApJ, 464, 943
Irwin, A. W. 2012, Astrophysics Source Code Library [record ascl:1211.002]
Itoh, N., Hayashi, H., Nishikawa, A., & Kohyama, Y. 1996, ApJS, 102, 411
Jermyn, A. S., Schwab, J., Bauer, E., Timmes, F. X., & Potekhin, A. Y. 2021, ApJ, 913, 72
Jermyn, A. S., Bauer, E. B., Schwab, J., et al. 2023, ApJS, 265, 15
Kupfer, T., Ramsay, G., van Roestel, J., et al. 2017a, ApJ, 851, 28
Kupfer, T., van Roestel, J., Brooks, J., et al. 2017b, ApJ, 835, 131
Kupfer, T., Bauer, E. B., Burdge, K. B., et al. 2020a, ApJ, 898, L25
Kupfer, T., Bauer, E. B., Marsh, T. R., et al. 2020b, ApJ, 891, 45
Kupfer, T., Bauer, E. B., van Roestel, J., et al. 2022, ApJ, 925, L12
Lagos, F., Schreiber, M. R., Parsons, S. G., Gänsicke, B. T., & Godoy, N. 2020, MNRAS, 499, L121
Lagos-Vilches, F., Hernandez, M., Schreiber, M. R., Parsons, S. G., & Gänsicke, B. T. 2024, MNRAS, 534, 3229
Langanke, K., & Martínez-Pinedo, G. 2000, Nucl. Phys. A, 673, 481
Lechien, T., de Mink, S. E., Valli, R., et al. 2025, ApJ, 990, L51
Liu, Z. W., Röpke, F. H., & Han, Z., 2023, Res. Astron. Astrophys., 23, 082001
Livne, E. 1990, ApJ, 354, L53
Livne, E., & Arnett, D. 1995, ApJ, 452, 62
Maxted, P. F. L., Heber, U., Marsh, T. R., & North, R. C. 2001, MNRAS, 326, 1391
Michaud, G., Richer, J., & Richard, O. 2007, ApJ, 670, 1178
Napiwotzki, R., Karl, C. A., Lisker, T., et al. 2004, Ap&SS, 291, 321
Nelemans, G., Preece, H., Temmink, K., Munday, J., & Pols, O. 2025, A&A, 700, A219
Neunteufel, P., Yoon, S. C., & Langer, N. 2019, A&A, 627, A14
Oda, T., Hino, M., Muto, K., Takahara, M., & Sato, K. 1994, At. Data Nucl. Data Tables, 56, 231
Ostrowski, J., Baran, A. S., Sanjayan, S., & Sahoo, S. K. 2021, MNRAS, 503, 4646
Paczynski, B. 1991, ApJ, 370, 597
Paxton, B., Bildsten, L., Dotter, A., et al. 2011, ApJS, 192, 3
Paxton, B., Cantiello, M., Arras, P., et al. 2013, ApJS, 208, 4
Paxton, B., Marchant, P., Schwab, J., et al. 2015, ApJS, 220, 15
Paxton, B., Schwab, J., Bauer, E. B., et al. 2018, ApJS, 234, 34
Paxton, B., Smolec, R., Schwab, J., et al. 2019, ApJS, 243, 10
Piersanti, L., Gagliardi, S., Iben, I., Jr., & Tornambé, A. 2003, ApJ, 598, 1229
Piersanti, L., Tornambé, A., & Yungelson, L. R. 2014, MNRAS, 445, 3239
Piersanti, L., Yungelson, L. R., & Bravo, E. 2024, A&A, 689, A287
Popham, R., & Narayan, R. 1991, ApJ, 370, 604
Potekhin, A. Y., & Chabrier, G. 2010, Contrib. Plasma Phys., 50, 82
Rajamuthukumar, A. S., Bauer, E. B., Justham, S., et al. 2025, A&A, 704, A82
Rodríguez-Segovia, N., Ruiter, A. J., & Seitenzahl, I. R. 2025, PASA, 42, e012
Rogers, F. J., & Nayfonov, A. 2002, ApJ, 576, 1064
Romero, A. D., Kepler, S. O., Joyce, S. R. G., Lauffer, G. R., & Córsico, A. H. 2019, MNRAS, 484, 2711
Ruiter, A. J., Belczynski, K., Benacquista, M., Larson, S. L., & Williams, G. 2010, ApJ, 717, 1006
Saumon, D., Chabrier, G., & van Horn, H. M. 1995, ApJS, 99, 713
Savonije, G. J., de Kool, M., & van den Heuvel, E. P. J. 1986, A&A, 155, 51
Schaffenroth, V., Pelisoli, I., Barlow, B. N., Geier, S., & Kupfer, T. 2022, A&A, 666, A182
Shen, K. J., & Bildsten, L. 2014, ApJ, 785, 61
Timmes, F. X., & Swesty, F. D. 2000, ApJS, 126, 501
Tokovinin, A., Thomas, S., Sterzik, M., & Udry, S. 2006, A&A, 450, 681
Tutukov, A. V., & Fedorova, A. V. 1989, Soviet Ast., 33, 606
Tutukov, A. V., & Yungelson, L. R. 1990, Soviet Ast., 34, 57
Vennes, S., Kawka, A., O'Toole, S. J., Németh, P., & Burton, D. 2012, ApJ, 759, L25
Wang, B. 2018, Res. Astron. Astrophys., 18, 049
Wang, B., & Han, Z. 2012, New Astron. Rev., 56, 122
Webbink, R. F. 1984, ApJ, 277, 355
Webbink, R. F. 2008, Astrophys. Space Sci. Lib., 352, 233
Woosley, S. E., & Kasen, D. 2011, ApJ, 734, 38
Yungelson, L. R. 2008, Astron. Lett., 34, 620
Zhang, Y., Li, Z., Chen, X., & Han, Z. 2024, ApJ, 977, 24
Zorotovic, M., & Schreiber, M. 2022, MNRAS, 513, 3587
Zorotovic, M., Schreiber, M. R., Gänsicke, B. T., & Nebot Gómez-Morán, A. 2010, A&A, 520, A86

Appendix A: Summary of Unsuccessful MESA Model Attempts

In this section, we present a summary of the parameter combinations that were explored but did not lead to viable models. The table lists the initial values adopted for each attempt and the specific reason why the simulation failed to produce an evolution consistent with our target scenario.

Table A.1. Summary of parameter combinations tested and the corresponding reasons for unsuccessful outcomes.

M1	M2	β	$P_{\rm orb}$ (d)	Reason for failure
3.5	2.7	0.25	1.8	Accretor overfills its Roche lobe; need lower M2 and smaller β.
2.301	2.300	0.40	50	He flash occurs before the end of stable mass transfer.
2.301	2.300	0.40	25	He flash occurs before the end of stable mass transfer.
2.301	2.300	0.40	10	He flash occurs before the end of stable mass transfer.
2.301	2.300	0.40	5	M2 too low.
2.301	2.300	0.30	4	Accretor overfills its Roche lobe.
2.31	2.29	0.20	4	Critical rotation problem.
2.31	2.30	0.20	5	Critical rotation problem.
2.51	2.50	0.40	10	Critical rotation problem.
2.51	2.50	0.40	25	Critical rotation problem.
2.501	2.500	0.40	25	Critical rotation problem.
2.501	2.500	0.50	50	He flash occurs before the end of stable mass transfer.
2.101	2.100	0.20	50	He flash occurs before the end of stable mass transfer.
2.101	2.100	0.20	10	He flash occurs before the end of stable mass transfer.
2.101	2.100	0.10	7	Mass-transfer rate too high ($\dot{M} > 10^{-2}$).
3.001	3.000	0.80	3	He flash with envelope too large; sdB mass too high; M2 not massive enough;
2.401	2.400	0.30	3	Critical rotation at M2 $\sim$ 3.60
2.401	2.400	0.35	4	Accretor overfills its Roche lobe.
2.401	2.400	0.35	5	Accretor overfills its Roche lobe.
2.401	2.400	0.35	3	Critical rotation (M2 $\sim$ 3.56).
2.401	2.400	0.25	3	Critical rotation; M2 core too small for massive WD.
2.501	2.500	0.25	3	Critical rotation (M2 $\sim$ 3.77); final $P_{\rm orb}$ only 166 d; M2 core too small.
2.501	2.500	0.15	3	Critical rotation (M2 $\sim$ 3.87); sdB mass OK; M2 core too small.
2.601	2.600	0.15	3	Critical rotation (M2 $\sim$ 4.0); sdB $T_{\rm eff}$ too low; M2 core insufficient.
2.701	2.700	0.15	3	Critical rotation (M2 $\sim$ 4.14); sdB parameters almost OK; M2 core still too small.
2.701	2.700	0.15	3	$T_{\rm eff}$ improves but $\log g$ and radius do not; accretor overfills its Roche lobe.
2.701	2.700	0.15	3.5	Accretor overfills its Roche lobe.
2.710	2.700	0.10	3	sdB parameters uncertain; accretor overfills its Roche lobe.